Survival and Apoptotic Pathways Initiated By TNF-α: Modeling and Predictions

Padmini Rangamani, Lawrence Sirovich

Laboratory of Applied Mathematics, Mount Sinai School of Medicine,
One Gustave L. Levy Place, New York, New York 10029; telephone: 212-659-1742;
e-mail: padmini.rangamani@mssm.edu

ABSTRACT: We present a mathematical model which includes TNF-α initiated survival and apoptotic cascades, as well as nuclear transcription of IκB. These pathways play a crucial role in deciding cell fate in response to inflammation and infection. Our model incorporates known specific protein–protein interactions as identified by experiments. Using these biochemical interactions, we develop a mathematical model of the NF-κB-mediated survival and caspase-mediated apoptosis pathways. Using mass action kinetics, we follow the formation of the survival and late complexes as well as the dynamics of DNA fragmentation. The effect of TNF-α concentration on DNA fragmentation is modeled and compares well with experiment. Nuclear transcription is also modeled phenomenologically by means of time lagged cytosolic concentrations. This results in transcription related concentrations undergoing under-damped oscillations, in qualitative and quantitative agreement with experiment. Using a tumor cell as a hypothetical model, we explore the interplay between the components of the survival and apoptotic pathways. Results are presented which make predictions on the limits of cellular oscillations in terms of time delay, initial concentration ratios and other features of the model. The model also makes clear predictions on cell viability in terms of DNA damage within the framework of TNF-α stimulus duration.

Biotechnol. Bioeng. 2007;97: 1216–1229.

© 2006 Wiley Periodicals, Inc.

KEYWORDS: mathematical modeling; TNF-α; NF-κB; apoptosis; caspase

Introduction

The immune system may be regarded as a complex network that is triggered in response to an external stimulus. This network is regulated to ensure that the cell can elicit an appropriate response to an invading pathogen or infection (Callard and Yates, 2005). Mathematical modeling of immune processes increases our understanding of the underlying biological function and processes. Theory, in the form of appropriate mathematical models forces us to organize existing information from experimental studies, and identifies the gaps in our understanding of the pathways. The process of model development should also factor in the suggestion of new experiments, which through verification and falsification (Popper, 2002) furnish insight into better understanding and modeling of the pathway.

A classic pathway of the immune system is the response of a cell to TNF-α. Binding of TNF-α to its receptor activates both the apoptotic and survival pathways. The outcome of the process depends on many factors, some of which are: duration and concentration of stimulus; activation of NF-κB; activation of the caspase cascade. Through mathematical modeling of the cellular response, we can hope to achieve a better understanding of this pathway which deals with the diametrically opposite fates of a cell.

The binding of TNF-α to its constitutive receptor TNFR1 and subsequent docking by adaptor proteins TRADD, TRAF2, and RIP-1 is well known (Barnhart and Peter, 2003; Baud and Karin, 2001). There is a general consensus on the sequence of events that lead to the activation of the transcription factor NF-κB by TNF-α via the interaction of these proteins with the IκB kinase IKK (Delhalle et al., 2004; Luo et al., 2005; Schneider and Tschopp, 2000; Schottelius et al., 2004), and the pathway has been consistently modeled (Cho et al., 2003a; Hoffmann et al., 2002; Lipniacki et al., 2004). Monte Carlo calculations for identifying the most sensitive interactions in the pathway are presented in Cho et al., (2003a), and models of the feedback regulatory loop of NF-κB activation module are presented in Hoffmann et al. (2002), Lipniacki et al. (2004), and Sung and Simon (2004). The feedback loop initiated by NF-κB leads to transcription

Correspondence to: P. Rangamani

of IκB[1] giving rise to a regulatory motif that determines the duration of response to TNF-α stimulation (Hoffmann et al., 2002). As a result of the delayed feedback loop, NF-κB translocates to the nucleus, where transcription takes place with a significant time delay. From the work of Hoffmann et al. (2002) and Nelson et al. (2004), we know that this can lead to under-damped oscillations of cytosolic concentrations. Because NF-κB activity is persistent in tumor cells, the simulational effects of small molecule inhibitors on pathway dynamics were studied in Sung and Simon (2004) and it was found that the system behaves differently depending on which molecule in the pathway is targeted. The cell-to-cell variability of NF-κB oscillations observed by Nelson et al. (2004) has been modeled along with the effect of extrinsic and intrinsic fluctuations in Hayot and Jayaprakash (2006). Mathematical models of death receptor-induced apoptosis have followed different approaches; Fussenegger et al. (2000) present a phenomenological model for apoptosis incorporating stress-induced and caspase-activated mechanisms based on evidence in the literature. The bistability characteristics of caspase-mediated apoptosis in a simplified model are presented in Eissing et al. (2004). This analysis showed the existence of an unstable steady state indicating the need for further control. A model for caspase-3 activation due to stimulation by Fas ligand and the effects of Bcl-2 effects on the pathway dynamics is developed in Hua et al. (2005).

In this article, we develop a mathematical model based on established protein–protein interactions that incorporates both the NF-κB and the apoptotic pathways and their interactions. In our model, we build on the framework for NF-κB activation as presented in Cho et al. (2003a) and incorporate a basic model of NF-κB-mediated transcription of IAP and IκB. The reactions for the apoptotic pathway are constructed from primary literature and involve specific interactions identified via experiments. With the inclusion of these interactions, the model takes on a degree of biological relevance, which allows exploration of the dynamics of the system and leads to predictions.

In a section dealing with mutant cases, we make a series of predictions based on this model. In addition, we make a range of predictions, chief amongst which are specific limits on when oscillations do and do not occur, and under which initial concentrations such oscillations appear. Another significant prediction concerns the dramatic effect that stimulus duration has on cell survival. It is hoped that this will engender experiments, the goal of which will be to attempt falsifications (Popper, 2002), and thus to begin the process by which a realistic model/theory can be accomplished.

---

[1]It is known that three isoforms IκB-α, β, ε figure in the cytosolic sequestration of NF-κB, and that NF-κB nuclear transcription results in IκB synthesis. In speaking of IκB we shall mean the IκB-α isoform. Modeling the other two isoforms is straightforward and we comment on this later.

TNF-α Biology

In this section, we present a summary of TNF-α biology that is relevant to the model development. TNF-α is a representative member of a family of cytokines involved in immunity and inflammation (Baud and Karin, 2001). Binding of TNF-α to its receptors can lead to the activation of NF-κB, a major transcription factor. NF-κB translocates to the nucleus and induces genes that can act to suppress apoptosis, caused by TNF-α-induced activation of the caspase cascade. Very low concentrations of TNF-α usually do not lead to apoptosis but higher concentrations of TNF-α induce shock like symptoms (Wajant et al., 2003). This phenomenon was recognized as an important balancing component in the outcome of TNF-α on virus infected cells versus healthy cells (Wallach, 1997). Thus, TNF-α plays a key role in regulating the choice between survival and apoptosis.

The fact that TNF-α can initiate more than one mode of action, at opposite extremes in cell fate, has been termed a "Sanhedrin verdict" (Wallach et al., 1998). The cell has a number of control and regulatory modules that ensure that an undue death pathway is not invoked. This also provides protection against low levels of cytokine activation by baseline noisy signals (McDunn and Cobb, 2005). From available evidence it is clear that TNF-α exerts a differential response that is dependent on tissue context, the amount and time of exposure to TNF-α and the type of receptor binding to the ligand (Wajant et al., 2003).

TNF-α exerts its effects by binding to its cognate receptors, belonging to the TNF receptor (TNFR) family. Among these, TNFR1 is constitutively expressed in most tissues. Binding of TNF-α to TNFR1 causes receptor trimerization and a conformation change (Baud and Karin, 2001). This allows for the binding and docking of death domain adaptor proteins (Baud and Karin, 2001). The recruitment of intracellular signaling molecules to the intracellular domain of TNFR1 occurs via adaptor proteins, which have no enzymatic activity of their own (Schottelius et al., 2004). The fact that the adaptor proteins TRADD, TRAF2, and RIP-1 are involved in complexes that initiate both the apoptotic and the anti-apoptotic pathway accounts for the experimental observation that as long as protein synthesis is not blocked, the cells can resist apoptosis by synthesizing IAP and related survival proteins (Wallach et al., 1998). The signaling mediated by TNFR1 is carried out by two sequential complexes (Micheau and Tschopp, 2003). Complex I or early complex contains the receptor and the adaptor proteins and leads to the activation of IKK and subsequently NF-κB. Complex II or the death-inducing signaling complex (DISC) does not contain the receptor but contains FADD and caspase-8 and leads to caspase-8 activation. The chronology of complex formation is noted in Micheau and Tschopp (2003). The apoptosis inhibition pathway is NF-κB dependent, and inhibition of NF-κB markedly increases apoptotic response to TNF-α. This molecular switch seems to depend on the intracellular

concentration of cell-signaling intermediates (McDunn and Cobb, 2005; Schottelius et al., 2004). NF-κB can play a cytoprotective role by expression of anti-apoptotic genes. IAPs are among these gene products and exert their influence by directly inhibiting the activity of caspases (Delhalle et al., 2004).

It has been suggested that this balance of cell life and death might provide a new approach to cancer therapy (Luo et al., 2005). NF-κB activation plays a critical role in the progression of tumors; inhibition of the survival pathway mediated by NF-κB may possibly lead to a desired cell death. Various steps of the activation pathway, including IKK activation, IκB phosphorylation and transport of NF-κB can be targeted by pharmacological agents. Thus, within this framework, inhibition of NF-κB may lead to a therapeutic approach in fighting a disease like cancer (Delhalle et al., 2004; Luo et al., 2005). Developing a comprehensive mathematical model for this pathway may provide us with a framework to investigate some of the pharmacological agents that help in fighting disease.

Model Development and Validation

By incorporating known direct protein–protein interactions, the TNF-α signal transduction model should yield a quantitative description of the sequence of events that take place upon ligand binding to its receptor TNFR1. The dynamics of the pathway depend on the interactions and reactions and thus provide a platform for experimental design. A wealth of quantitative temporal/biochemical information emerges from model simulation, which on comparison with experiment can lead to model improvement. We present below, the elements of the pathway, in terms of four linked modules. The full set of reactions is shown as four modules in Table I, with species/concentration relations given in Table II. A biochemical flow diagram is presented in Figure 6, and the resulting dynamical system is constructed in the Appendix.

Module 1: The Early Complex

Binding of TNF-α to TNFR1 leads to the recruitment of the death domain proteins TRADD, TRAF2, and RIP-1 to the ligand-receptor complex. These proteins form the multi-protein complex called the early complex (Micheau and Tschopp, 2003), which is required for the downstream activities. The rates of association and dissociation for this and other complexes are based on the values used in Cho et al. (2003a) and Sung and Simon (2004). The binding rates are assumed to be similar for all the adaptor proteins. The early complex, the concentration of which is represented by c_9, forms the pedestal for the two sub-pathways—(1) transcription factor NF-κB production; (2) induction of enzymatic caspase cascade.

Module 2: Activation of NF-κB

NF-κB is sequestered in inactive form in the cytoplasm through the interaction with inhibitory proteins, the IκBs. Proteolytic degradation of IκB immediately precedes, and is required for, NF-κB release and subsequent nuclear translocation (Greten and Karin, 2004). The inactive inhibitory kinase IKK binds to the early complex, forming a survival complex (c_{11}). Dissociation of this complex leads to activation of IKK and regeneration of the adaptor

Table I. Reactions involved in the pathway.

Module 1: formation of the early complex	
TNF-α + TNFR1 ⇔ TNF-α/TNFR1	$J_1 = k_1 \cdot c_1 \cdot c_2 - k_2 \cdot c_3$
TNF-α/TNFR1 + TRADD ⇔ TNF-α/TNFR1/TRADD	$J_2 = k_3 \cdot c_3 \cdot c_4 - k_4 \cdot c_5$
TNF-α/TNFR1/TRADD + TRAF2 ⇔ TNF-α/TNFR1/TRADD/TRAF2	$J_3 = k_5 \cdot c_5 \cdot c_6 - k_6 \cdot c_7$
TNF-α/TNFR1/TRADD/TRAF2 + RIP-1 ⇔ TNF-α/TNFR1/TRADD/TRAF2/RIP-1	$J_4 = k_7 \cdot c_7 \cdot c_8 - k_8 \cdot c_9$
Module 2: activation of NF-κB by the multi-protein complexes	
TNF-α/TNFR1/TRADD/TRAF2/RIP-1 + IKK ⇔ TNF-α/TNFR1/TRADD/TRAF2/RIP-1/IKK	$J_5 = k_9 \cdot c_{10} \cdot c_9 - k_{10} \cdot c_{11}$
TNF-α/TNFR1/TRADD/TRAF2/RIP-1/IKK ⇒ TNFR1 + TRADD + TRAF2 + RIP-1 + IKK*	$J_6 = k_{11} \cdot c_{11}$
IKK* + IκB/NF-κB ⇔ IκB/NF-κB/IKK*	$J_7 = k_{12} \cdot c_{12} \cdot c_{13} - k_{13} \cdot c_{14}$
IκB/NF-κB/IKK* ⇒ IKK + IκB-P + NF-κB	$J_8 = k_{14} \cdot c_{14}$
Module 3: activation of caspases by multi-protein complexes	
TNF-α/TNFR1/TRADD/TRAF2/RIP-1 + FADD ⇔ TNF-α/TNFR1/TRADD/TRAF2/RIP-1/FADD	$J_9 = k_{15} \cdot c_9 \cdot c_{17} - k_{16} \cdot c_{18}$
TNF-α/TNFR1/TRADD/TRAF2/RIP-1/FADD ⇒ TRADD/TRAF2/RIP-1/FADD + TNFR1	$J_{10} = k_{17} \cdot c_{18}$
TRADD/TRAF2/RIP-1/FADD + caspase-8 ⇔ TRADD/TRAF2/RIP-1/FADD/caspase-8	$J_{11} = k_{18} \cdot c_{19} \cdot c_{20} - k_{19} \cdot c_{21}$
TRADD/TRAF2/RIP-1/FADD/caspase-8 ⇒ caspase-8* + TRADD + FADD + RIP-1 + TRAF2	$J_{12} = k_{20} \cdot c_{21}$
Caspase-8* + caspase-3 ⇔ caspase-8*/caspase-3	$J_{13} = k_{21} \cdot c_{22} \cdot c_{23} - k_{22} \cdot c_{24}$
Caspase-8*/caspase-3 ⇒ caspase-3* + caspase-8*	$J_{14} = k_{23} \cdot c_{24}$
Module 4: nuclear activity	
Caspase-3* + DNA ⇔ caspase-3*/DNA	$J_{15} = k_{24} \cdot c_{25} \cdot c_{29} - k_{25} \cdot c_{30}$
Caspase-3*/DNA ⇒ DNA-fragmentation + Caspase-3*	$J_{16} = k_{26} \cdot c_{30}$
NF-κB ⇒ c-IAP + IκB	$J_{17} = p \cdot c_{16} \, (t - \tau)$
Caspase-3* + c-IAP ⇒ caspase-3*/c-IAP	$J_{18} = k_{28} \cdot c_{27} \cdot c_{25}$
IκB + NF-κB ⇒ IκB/NF-κB	$J_{19} = k_{29} \cdot c_{16} \cdot c_{31}$

Table II. Differential equations governing the reaction rates of reactions shown in Table I.

$$\frac{dc_1}{dt} = -k_1 \cdot c_1 \cdot c_2 + k_2 \cdot c_3$$

$$\frac{dc_2}{dt} = -k_1 \cdot c_1 \cdot c_2 + k_2 \cdot c_3 + k_{17} \cdot c_{18} + k_{11} \cdot c_{11}$$

$$\frac{dc_3}{dt} = k_1 \cdot c_1 \cdot c_2 - k_2 \cdot c_3 - k_3 \cdot c_3 \cdot c_4 + k_4 \cdot c_5$$

$$\frac{dc_4}{dt} = -k_3 \cdot c_3 \cdot c_4 + k_4 \cdot c_5 + k_{11} \cdot c_{11} + k_{20} \cdot c_{21}$$

$$\frac{dc_5}{dt} = k_3 \cdot c_3 \cdot c_4 - k_4 \cdot c_5 - k_5 \cdot c_5 \cdot c_6 + k_6 \cdot c_7$$

$$\frac{dc_6}{dt} = -k_5 \cdot c_5 \cdot c_6 + k_6 \cdot c_7 + k_{11} \cdot c_{11} + k_{20} \cdot c_{21}$$

$$\frac{dc_7}{dt} = k_5 \cdot c_5 \cdot c_6 - k_6 \cdot c_7 - k_7 \cdot c_7 \cdot c_8 + k_8 \cdot c_9$$

$$\frac{dc_8}{dt} = -k_7 \cdot c_7 \cdot c_8 + k_8 \cdot c_9 + k_{11} \cdot c_{11} + k_{20} \cdot c_{21}$$

$$\frac{dc_9}{dt} = k_7 \cdot c_7 \cdot c_8 - k_8 \cdot c_9 - k_9 \cdot c_9 \cdot c_{10} + k_{10} \cdot c_{11} - k_{15} \cdot c_9 \cdot c_{17} + k_{16} \cdot c_{18}$$

$$\frac{dc_{10}}{dt} = -k_9 \cdot c_9 \cdot c_{10} + k_{10} \cdot c_{11} + k_{14} \cdot c_{14}$$

$$\frac{dc_{11}}{dt} = k_9 \cdot c_9 \cdot c_{10} - k_{10} \cdot c_{11} - k_{11} \cdot c_{11}$$

$$\frac{dc_{12}}{dt} = -k_{12} \cdot c_{12} \cdot c_{13} + k_{13} \cdot c_{14} + k_{11} \cdot c_{11}$$

$$\frac{dc_{13}}{dt} = -k_{12} \cdot c_{12} \cdot c_{13} + k_{13} \cdot c_{14} + k_{29} \cdot c_{16} \cdot c_{31}$$

$$\frac{dc_{14}}{dt} = k_{12} \cdot c_{12} \cdot c_{13} - k_{13} \cdot c_{14} - k_{14} \cdot c_{14}$$

$$\frac{dc_{15}}{dt} = k_{14} \cdot c_{14}$$

$$\frac{dc_{16}}{dt} = k_{14} \cdot c_{14} - k_{29} \cdot c_{16} \cdot c_{31}$$

$$\frac{dc_{17}}{ct} = -k_{15} \cdot c_9 \cdot c_{17} + k_{16} \cdot c_{18} + k_{20} \cdot c_{21}$$

$$\frac{dc_{18}}{dt} = k_{15} \cdot c_9 \cdot c_{17} - k_{16} \cdot c_{18} - k_{17} \cdot c_{18}$$

$$\frac{dc_{19}}{ct} = k_{17} \cdot c_{18} - k_{18} \cdot c_{19} \cdot c_{20} + k_{19} \cdot c_{21}$$

$$\frac{dc_{20}}{dt} = -k_{18} \cdot c_{19} \cdot c_{20} + k_{19} \cdot c_{21}$$

$$\frac{dc_{21}}{dt} = k_{18} \cdot c_{19} \cdot c_{20} - k_{19} \cdot c_{21} - k_{20} \cdot c_{21}$$

$$\frac{dc_{22}}{dt} = k_{20} \cdot c_{21} - k_{21} \cdot c_{22} \cdot c_{23} + k_{22} \cdot c_{24} + k_{23} \cdot c_{24}$$

$$\frac{dc_{23}}{dt} = -k_{21} \cdot c_{22} \cdot c_{23} + k_{22} \cdot c_{24}$$

$$\frac{dc_{24}}{dt} = k_{21} \cdot c_{22} \cdot c_{23} - k_{22} \cdot c_{24} - k_{23} \cdot c_{24}$$

$$\frac{dc_{25}}{dt} = k_{23} \cdot c_{24} - k_{28} \cdot c_{27} \cdot c_{25} - k_{24} \cdot c_{29} \cdot c_{25} + k_{25} \cdot c_{30} + k_{26} \cdot c_{30}$$

$$\frac{dc_{26}}{dt} = k_{26} \cdot c_{30}$$

$$\frac{dc_{27}}{dt} = p \cdot c_{16}(t - \tau) - k_{28} \cdot c_{27} \cdot c_{25}$$

$$\frac{dc_{28}}{dt} = k_{28} \cdot c_{27} \cdot c_{25}$$

$$\frac{dc_{29}}{dt} = -k_{24} \cdot c_{29} \cdot c_{25} + k_{25} \cdot c_{30}$$

$$\frac{dc_{30}}{dt} = k_{24} \cdot c_{29} \cdot c_{25} - k_{25} \cdot c_{30} - k_{26} \cdot c_{30}$$

$$\frac{dc_{31}}{dt} = p \cdot c_{16}(t - \tau) - k_{29} \cdot c_{16} \cdot c_{31}$$

proteins. The phosphorylation of IκB and release of NF-κB is mediated by the activated IKK. The rate constants for IKK activation and NF-κB release are based on the work by Hoffmann et al. (2002).

Module 3: Activation of the Caspase Cascade

Caspases are central in activating the apoptotic machinery. Caspases are generally divided into two categories— initiator caspases and effector caspases. The early complex (c_9) when bound to FADD and then procaspase-8, leads to activation of the apoptotic signaling machinery via the DISC, c_{21}. Experimental evidence for these complexes can be found in Micheau and Tschopp (2003) and Shi (2002). DISC consists of FADD and caspase-8 in addition to TRADD and TRAF2 but not TNFR1 (Micheau and Tschopp, 2003; Shi, 2002). Therefore, an additional reaction is included in Module 3 of Table I to depict the formation of DISC without TNFR1. DISC releases active caspase-8 which

is now capable of activating the effector, caspase-3. The dynamics of caspases 8 and 3 is presented in Wang et al. (2005), and the rate constants were chosen to match the experimental evidence provided in Hua et al. (2005).

Module 4: Nuclear Activity

NF-κB is a transcription factor and its release is an irreversible step in the signaling pathway and constitutes a commitment to transcription. NF-κB, in the nucleus binds to DNA and leads to the transcription of inhibitor of apoptosis protein (IAP) and IκB among others. c-IAP inhibits apoptosis by specifically binding to activated caspase-3 and thus preventing DNA fragmentation (Holcik and Korneluk, 2001; Liston et al., 1997). Although c-IAP binding to caspase-3[*] is not nuclear activity, we include it in this module because of the delay term. The model IκB transcription rates follow that used in Hoffmann et al. (2002) and Sung and Simon (2004), with similar values for transcription rates for IAP.

Construction of the Model

Each of the steps outlined in the modules above is a complex biological interaction. The formulation of the model involves binding reactions between ligand and receptor, protein–protein interactions, and enzymatic reactions. Release of transcription factors leads to transcription and associated transport processes. Accounting for all these steps makes for a very complex model.

A detailed transcriptional model of IκB transcription by NF-κB has been developed in Hoffmann et al. (2002) and further developed in Nelson et al. (2004). Here we chose to take a simpler dynamical systems approach that allows us to study the dynamics of the system. Instead of treating the nucleus and cytosol as separate compartments, transport processes are subsumed into the kinetic rate constants and the transcription process is represented as a delayed reaction. For simplification of analysis, all reactions are represented as mass action processes. We represent the complex transport process and transcription machinery involving NF-κB which consists of multiple steps, in a single reaction; represented by the flux J_{17} in Table I. This simplification allows us to replace a complicated mechanism by a simpler phenomenological one. The chosen delay time used for transcription is 20 min, as suggested in Sung and Simon (2004).

Apoptosis is a binary event and is characterized by the presence of DNA laddering. Our model monitors the extent of this DNA damage as an indication of the extent of apoptosis (Ioannou and Chen, 1996). Active caspase-3 activates a DNase named caspase activated DNase (CAD) by cleaving its associated inhibitor ICAD (inhibitor of CAD) (Jin and El-Deiry, 2005). The free DNase can act on DNA, cleaving it at the linker regions, thus resulting in DNA laddering. In the spirit of simple modeling, we represent this

multi-step pathway phenomenologically by two reactions whereby caspase-3[*] acts on intact DNA and then fragments it (fluxes J_{15} and J_{16} in Table I). We assume that about 1% of the total genomic DNA is present in linker DNA and that this is the available target for caspase-3[*]. This appears as the initial concentration of intact DNA (c_{29}) in Table II. The concentration of available DNA sites that have been cleaved is noted as fragmented DNA and can be followed as a marker for apoptosis, and also monitors the level of caspase-3[*] that is present. Because we are studying single cell dynamics in our model, we refer to the idea of DNA fragmentation as a measure of damage inflicted by TNF-α. These ideas are supported by the quantitation of DNA fragmentation as presented in Ioannou and Chen (1996).

The initial values for the different species are set based on values used in previous studies (Cho et al., 2003b; Eissing et al., 2004; Hoffmann et al., 2002). The initial value for intact DNA is calculated by assuming that 1% of the entire human genome (6.4×10^9 base pairs) is available as linker DNA and therefore susceptible to fragmentation due to the action of effector caspase. Fragmented DNA in this case is defined as the fraction of intact DNA sites that have been attacked by the activity of caspase. We use an average molecular weight of 660 g/mol/bp to convert the number of base pairs of DNA to moles. The volume of the cell is calculated as a sphere with a diameter of 50 μm. An explicit mathematical model based on the above modules, and related deliberations appear in the Appendix.

Results

The consequences of TNF-α binding to TNFR-1 can be pursued using the model and we can follow the time histories of all the concentrations involved in the pathway. Additionally, by reasonably modifying protein concentrations, we can predict some results that may be used to develop experimental strategies and lead to refinements of the model. All simulations described below are run for the nominal time period of 6 h, to enable direct comparison with standard practice in published experimental work. The case of a 6 h threshold, which conforms to experimental practice, was also chosen as a reasonable period beyond which mechanisms not included in the model might take effect.

Sensitivity to TNF-α Stimulation

Initial simulations were carried out to validate the model against experimental observations by qualitative comparisons of dynamics of important components. In response to increasing concentrations of TNF-α as seen in Figure 1a and b, the formation of the survival complex, complex I in Micheau and Tschopp (2003) happens earlier than the death complex, complex II in Micheau and Tschopp (2003). This early formation of complex I, roughly within 30 min, and the formation of complex II, at roughly 60 min, is in
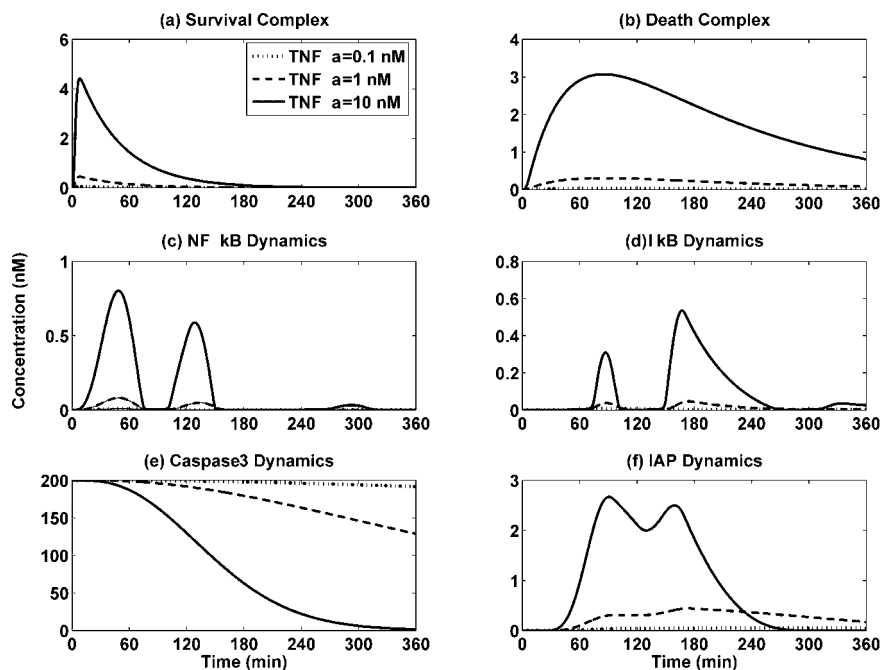
Figure 1. Sensitivity to TNF-α simulation. The dynamics of the pathway components to simulation by TNF-α at 0.1, 1, 10 nM are shown. Subparts (**a**) and (**b**) show the time profiles for the formation of the survival and death complexes as identified in Micheau and Tschopp (2003). Subpart (**c**) shows the dynamics of free NF-κB which leads to the transcription of IκB (**d**). Activation of caspase-3 and IAP formation are shown in (**e,f**) respectively. The simulations are carried out for 6 h to enable direct comparison with experiment (Hoffmann et al., 2002).

qualitative agreement with the Western blot experiments of Micheau and Tschopp (2003).

As TNF-α concentration increases, the maximum concentration of these complexes also increases, indicating that the system is sensitive to stimulation levels. In response to increasing concentrations of TNF-α, activation of NF-κB and IKK increase in agreement with Hoffmann et al. (2002) and Kearns et al. (2006). As seen in Figure 1c, activation of NF-κB results in delayed transcription and leads to oscillatory behavior as the concentration of TNF-α increases, in agreement with Hoffmann et al. (2002) and Nelson et al. (2004). This directly affects the dynamics of IκB, Figure 1d, and the results are consistent with experimental observations (Kearns et al., 2006) where the sensitivity to TNF-α treatment is shown. Our simple delay model shows a secondary IκB peak larger than the first, contrary to Hoffmann et al. (2002) and experiments; however, we have not included the damping effect of IκBβ and IκBε in the model, both of which produce damping (Barken et al., 2005). As seen in Figure 1e, caspase-3 exhibits a delay of ~30 minutes before being activated, consistent with the observed results of Rehm et al. (2002) and Wang et al. (2005). A prediction of the model is that in response to oscillations in NF-κB dynamics, the profile for IAP dynamics exhibits a corresponding under-damped oscillation, Figure 1f.

DNA Fragmentation

DNA fragmentation is a hallmark of the onset of apoptosis. The dynamics of DNA fragmentation for the apoptotic and full pathway is shown in Figure 2a. With TNF-α increase, the rate and amount of caspase-3 cleavage increases. As mentioned earlier, DNA fragmentation dynamics, shown in Figure 2a, monitors production of caspase-3*. The apoptotic cascade can be turned off by setting the initial concentration of FADD to zero. In the absence of the apoptotic cascade, no DNA fragmentation will appear. This result is in accordance with experimental observations that cells mutant in the caspase pathway lose their ability to initiate apoptosis, even when large quantities of cytokines are used (Delhalle et al., 2004; Karin et al., 2004). In Figure 2a, we see that in the absence of the anti-apoptotic pathway (only the apoptotic pathway is active since the initial concentration of IKK is set to zero), the rate of DNA fragmentation is faster and for large concentration of TNF-α (10 nM), most of the DNA is fragmented after 6 hours. These results are in qualitative agreement with observations that TNF-α-induced apoptosis is faster when the IKK pathway is not fully functional (Micheau and Tschopp, 2003). When both pathways are active, we see that the DNA fragmentation is diminished and the process takes longer (Fig. 2a), possibly allowing time for other genes to come into play (see Future Directions Section).

Stimulation of cells in vitro using TNF-α is known to initiate both the activation of NF-κB and the apoptotic cascade (Barnhart and Peter, 2003). More importantly, the amount of DNA damage is known to increase with the amount of TNF-α used (or released in vivo) (Wajant et al., 2003). Figure 2b shows the effect of increasing TNF-α concentration on DNA damage 6 h after stimulation. The sigmoidal shape of the curve captures the typical dose-response curve in the absence of competition, indicating the response of the cell to increasing stimulation by TNF-α. At low concentration of TNF-α (10^{-4} to 1 nM), there is very little total DNA damage induced by TNF-α. On increasing the concentration of TNF-α beyond 1 nM, there is more DNA damage and on using larger concentrations of TNF-α (10–100 nM), there is complete DNA damage after 6 h.

Effect of Stimulus Duration

We also explored the effect of finite stimulus duration. The circles in Figure 2b represents total DNA fragmentation after 6 h, given a 1 nM initial spike (δ-function) of TNF-α. This location was chosen because of its proximity to the inflection point of the sigmoidal curve described in the previous paragraph. In a series of explorations, we examined the degree of DNA fragmentation if this same initial spike of TNF-α is spread uniformly over durations of 2, 10, and 60 min. The results of this are indicated by $*$, $\bullet$, and $\star$ respectively in Figure 2b. As is clear from the figure, even a 2 min duration leads to a significant reduction of DNA fragmentation after 6 h, and that a 10 min, and hence a 60 min duration have profound effects. Because the amount of DNA fragmentation in these last two instances is very small, we may consider that the cell has survived.

Effect of Varying IKK and FADD Levels

IKK and FADD play a pivotal role in activating the anti-apoptotic and apoptotic pathways, respectively. The binding of one of these two adaptor proteins to the early complex is the determinant of the pathway that is activated. FADD dominant negative mutants showed no change in cell viability, indicating that the apoptosis cascade was not activated (Micheau and Tschopp, 2003). FADD knockouts resulted in impaired TNF-α-induced apoptosis while IKK knockouts resulted in impaired NF-κB activation (Wajant et al., 2003). Therefore, it is clearly of interest to explore the effects of different expression levels of these two proteins within the current framework by means of mutant studies. We consider the effects of changing the expression of these two proteins on the dynamics of the components of the survival and apoptotic pathways. TNF-α, the customary control, was taken at the above reference value of 1 nM for these simulations.

IKK levels were varied from the baseline value of 100 nM to 1, 10, and 1,000 nM (Fig. 3). For low amounts of IKK (1 and 10 nM), we see that caspase-3 activity is higher, with the apoptotic pathway showing more activity than the survival
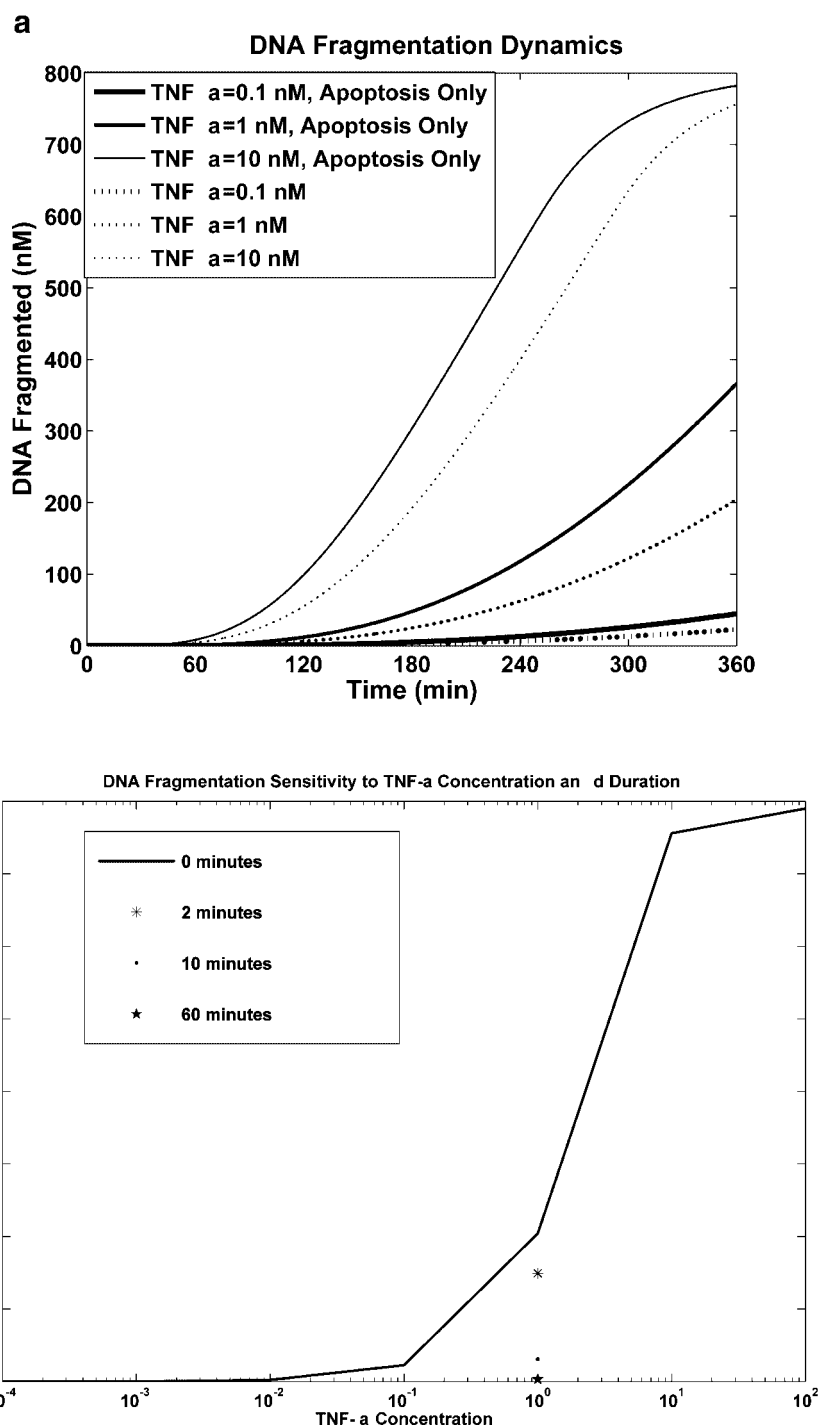
Figure 2. DNA fragmentation in response to TNF-α stimulation. **a**: DNA fragmentation dynamics for three different values of TNF-α stimulation (0.1, 1, 10 nM) for the apoptosis only pathway (setting IKK initial to zero) and full pathway is shown. The rate of DNA fragmentation is faster for the apoptosis only pathway when compared to the full pathway for the same level of TNF-α used. Subpart (**b**) shows the dose response curve of DNA fragmentation in response to stimulation by different levels and durations of TNF-α. The curve follows a typical sigmoidal shape.

pathway (Fig. 3e). By contrast, when the amount of IKK is increased to 1,000 nM, we see a decrease in the formation of the death complex and an increase in the formation of survival complex (Fig. 3a). At 1 and 10 nM of IKK,

oscillatory dynamics for NF-κB and IκB are not observed, but are observed for 100 and 1,000 nM concentrations of IKK, Figure 3c and d, indicating the dependence of the negative feedback loop on IKK levels. Increase in IKK leads
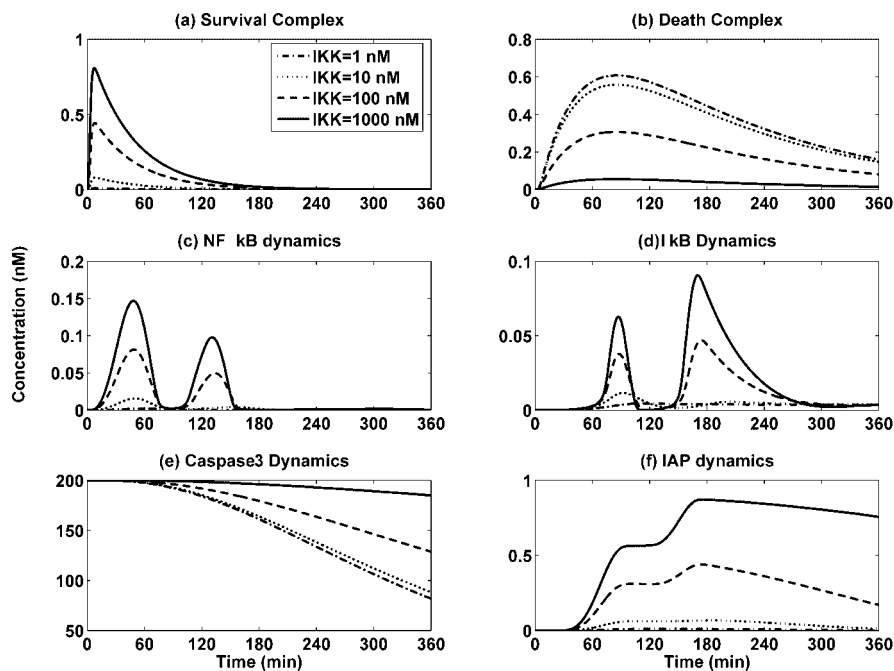
Figure 3. Effect of IKK levels on system components. The same pathway components as shown in Figure 1 for 1 nM TNF-α stimulation and different values of IKK are shown. As IKK expression level increases, the survival pathway dominates increases the oscillatory feedback behavior of NF-κB and IκB. As a result, caspase-3 activation rate decreases.

to decreased caspase-3 cleavage as seen in Figure 3e. IAP dynamics shows corresponding behavior with increasing levels of IKK, pointing to increased survival potential in the presence of increased IKK (Fig. 3f). FADD levels were similarly varied from the baseline value of 100 nM to 1, 10, and 1,000 nM (Fig. 4). An increase in the amount of death complex formed and decrease in the formation of survival complex formed were observed (Fig. 4a and b). The oscillatory dynamics of NF-κB and IκB are virtually lost for large values of FADD (1,000 nM) indicating that the apoptotic pathway has a stronger downstream effect in this case. As the concentration of FADD increases, caspase-3 cleavage rate increases and IAP formation rate decreases (Fig. 4e and f).

Increasing concentration of IKK increases amplitude of oscillations in NF-κB and IκB. On induction of oscillatory behavior, IAP production increases and caspase-3 activity decreases (Fig. 3). By contrast, decreasing FADD concentration induces oscillatory behavior. Loss of oscillations increases caspase-3 activity rates (Fig. 4). In addition, as noted in the literature (Holcik and Korneluk, 2001; Liston et al., 1997), the survival capabilities induced by IKK and NF-κB are stronger than the apoptotic capabilities. The results from the mutant studies are in agreement with the phenotype observed in experiments. These results may have implications for tumor cells and initiating apoptotic processes in them. By overexpressing the components of the apoptotic machinery, it may be possible to induce apoptosis in tumorigenic cells, and prevent tumor growth/spreading. The possibility of such mutant effects offers an attractive

potential for inducing apoptosis in tumorigenic cells. Tumor cells, in most cases, have some damage to their apoptotic machinery, thus immortalizing them (Luo et al., 2005). It is presently only a hope that this pathway can be modified with gene therapies and other genetic advancements. A combination of increasing the amount of FADD expression and decreasing the amount of IKK rather than targeting each pathway individually may prove to be more beneficial.

Thresholds of Oscillation

We also explored the appearance of oscillations with respect to the initial concentrations of IKK and FADD. For the nominal case of a 20 min delay, discussed above, we learned that oscillations do not appear if the ratio of initial concentrations, [FADD]/[IKK] is greater than 11.11 and that oscillations always appear for all values of the ratio less than 11.11. This is indicated by an inset in Figure 5. The fact that this is a straight line has an analytical basis; however this is beyond the present scope of the article.

These results naturally depend on the parameters of the problem; however the most important determinant is the delay time itself. In fact, for the nominal case of [FADD]/[IKK] ratio being 1, there are no oscillations for delay times less than 5 minutes, nor greater than 30 minutes. With this in mind, we also explored effect of delay time on the presence or absence of oscillations as a function of the ratio of initial concentrations. This is summarized in Figure 5. For
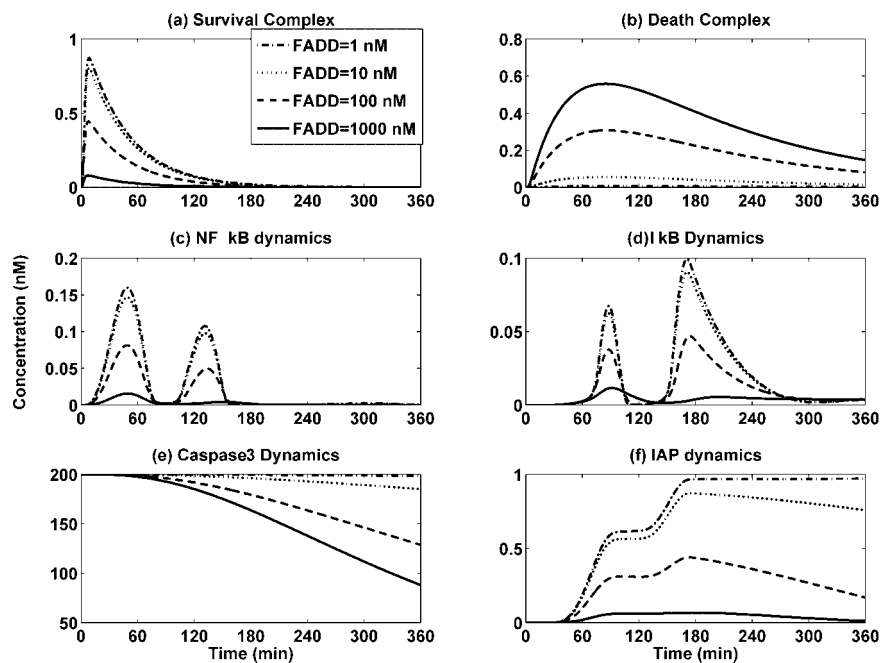
Figure 4. Effect of FADD levels on system components. The same pathway components as shown in Figure 1 for 1 nM TNF-α stimulation and different values of FADD are shown. Increase in FADD concentration leads to a decrease in NF-κB and IκB oscillation behavior as predicted by the model. IAP transcription decreases and caspase-3 activation rate increases.

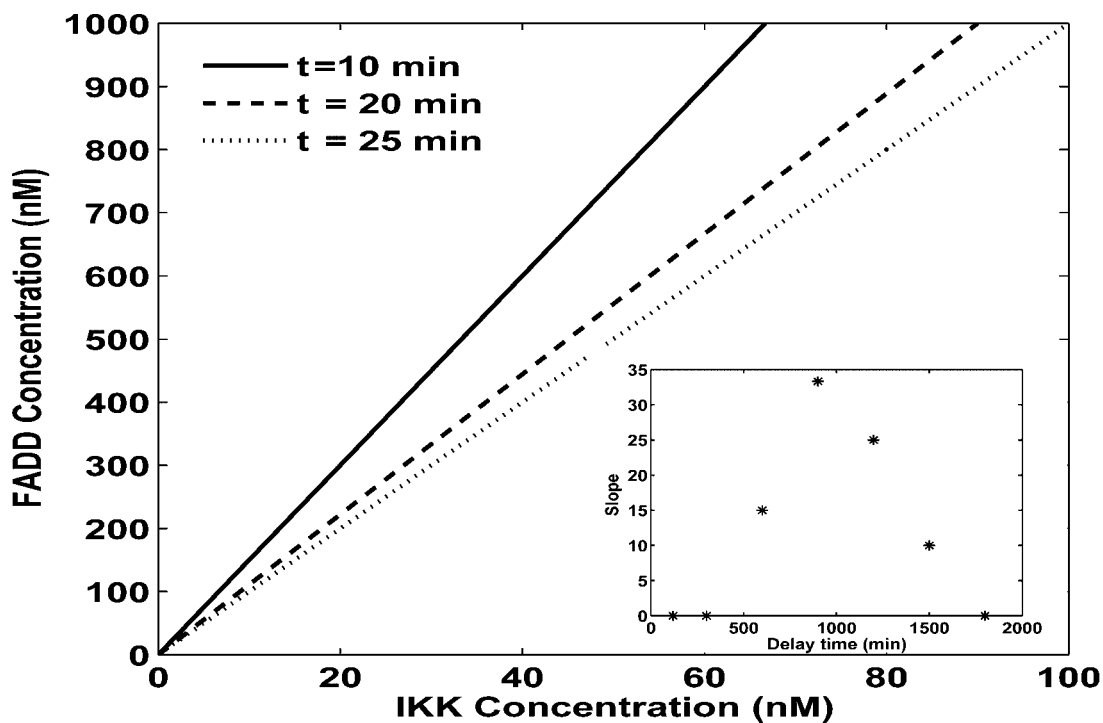**Figure 5.** Thresholds of oscillations. The presence or absence of oscillations with respect to the ratio of initial concentrations of FADD and IKK and the transcription delay time are shown. Inset shows the variation of slope with the delay time.
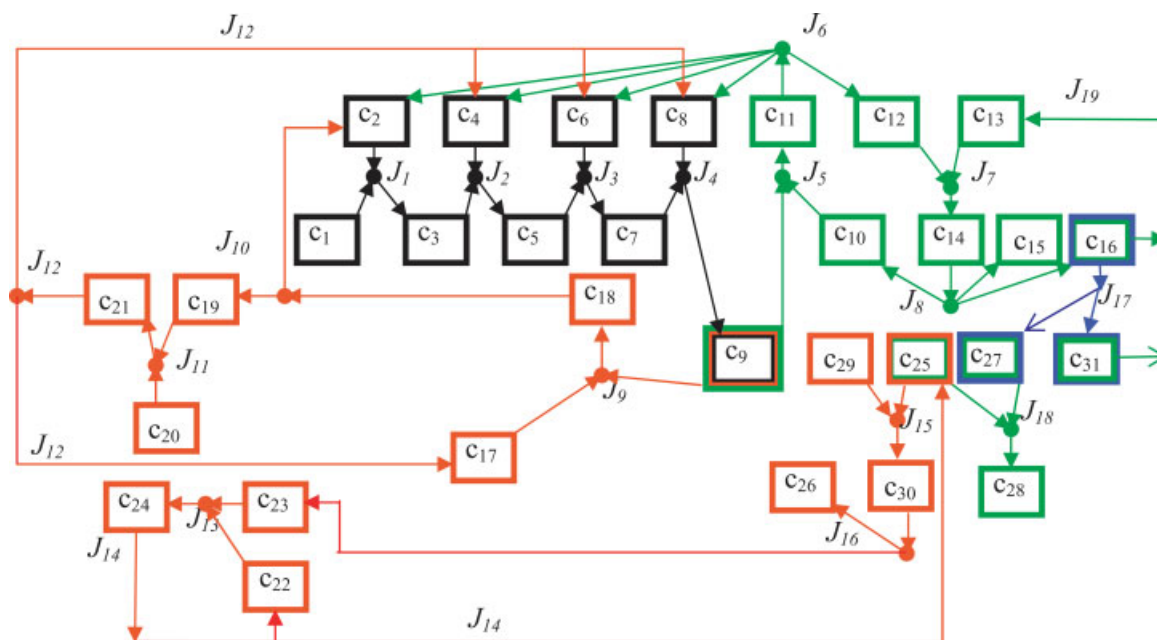
Figure 6. The biochemical pathway showing the interaction of different components in the pathway. The reactions in Module 1 shown in Table I are shown in black; the reactions in Module 2 are shown in green, and Module 3 in red. Components shared between the apoptotic and anti-apoptotic pathways (c_9, c_{25}) are boxed in multiple colors. Transcription mechanisms are colored blue.

each of the delay times indicated in Figure 5, we found a straight line slope in the FADD versus IKK plane above which no oscillations exist and below which oscillations always exist. The slopes of these lines are indicated in the insert at the lower right.

Discussion

We have assembled a mathematical model for the biochemical reactions initiated by TNF-α binding to its constituent receptor TNFR1. The reactions represent the apoptotic and the anti-apoptotic pathways initiated by this cytokine. The model captures the dynamics of the formation of the survival and death complexes which play an important role in the activation of the anti-apoptotic and apoptotic pathways. The effect of the individual sub-pathways and the full pathway on DNA fragmentation reiterates the importance of the role played by the survival pathway in helping a cell fight possible cytotoxic effects of TNF-α. The response of cells to TNF-α is tissue and context dependent. Very low levels of TNF-α (10^{-4} nM) can be assumed to be baseline or noise, since physiologic concentrations of TNF-α lie in the range of 0.6 nM (10 ng/mL). At such concentrations, the survival pathway, in conjunction with other pathways like the JNK pathway, is known to favor cell survival by the induction of anti-apoptotic genes (Papa et al., 2004). Most in vitro experiments use concentrations of TNF-α in the range of

10–100 ng/mL (0.6–6 nM) (Micheau and Tschopp, 2003). The sensitivity of cells to TNF-α concentration has been studied under different experimental conditions in different cell lines, (Polunovsky et al., 1994; Wang et al., 1996; Wright et al., 1992). Apoptosis is observed in these conditions in the presence of cycloheximide, an inhibitor of protein synthesis or mutants in IκB, because IAP cannot be synthesized (Micheau and Tschopp, 2003; Wajant et al., 2003; Wright et al., 1992). While the experimental conditions differ in all these studies, there seems to be general agreement on the effect of increasing concentration of TNF-α on apoptosis. As the amount of TNF-α increases beyond 0.6 nM (10 ng/mL), there is an increase in the percentage of apoptotic cells. Figure 2b captures a similar trend, indicating that the model respects the behavior observed in experiments.

We analyzed the response of the TNFR1 pathway to the different levels of expression of apoptotic proteins (e.g., FADD) or knockdown of survival proteins (e.g., IKK). In this analysis, a goal has been elucidation of the interplay between the survival and apoptotic pathways response to increased levels of component proteins. To this end, we varied the expression levels of IKK and FADD. The oscillatory feedback behavior of NF-κB, IKK, and IκB that has been experimentally observed depends on the concentration of IKK and FADD. By increasing the levels of FADD, we observe the loss of the oscillatory feedback loop and increasing caspase-3* cleavage, indicating that the apoptotic pathway negatively regulates the survival pathway. The reverse effect is seen by increasing the concentrations of IKK, whence oscillations

begin to set in and caspase-3* cleavage rate decreases. Whether these data indicate that the negative feedback loop associated with NF-κB plays any role other than attenuation of NF-κB levels appears to be debatable (Barken et al., 2005; Nelson et al., 2005). It should be noted that modest oscillatory behavior is present at the nominal level of TNF-α, 1 nM, but even at this level, "mutant" levels of IKK and FADD produce enhanced oscillations, Figures 3 and 4.

The negative feedback mechanism established by IκB has been experimentally observed to play an important role in the attenuation of NF-κB signaling (Hoffmann et al., 2002; Kearns et al., 2006). These computational models of oscillatory behavior have captured the experimental observations. We have used a simpler approach to capture this essential behavior. It has been observed that the α isoform of IκB exhibits oscillatory behavior and the ε isoform exhibits delayed transcription relative to the α isoform, resulting in two negative feedback loops. In the current model, we have succeeded in capturing the dynamics of the α isoform and analyzing the effect of oscillations on the apoptotic pathway and caspase activation. The oscillations observed in the delayed response of IκB-ε can be obtained in our model using longer delay times. If a certain isoform does not exhibit oscillations, then the delay time can be set to zero. Using our model, we can study the different isoforms (or include additional isoforms, see Future Directions Section) by using different delay times, thus providing a mathematical framework to study subtly different problems with the same network architecture.

Mathematical modeling of the TNF-α initiated survival and apoptotic pathways allows us to organize available experimental data and study effects of various parameters. In this case, we study the effect of expression levels of component proteins in the apoptotic and survival pathways. Simulations based on this model can be used to analyze multivariable experiments and predicts interactions between components. We conclude this section with a brief summary of predictions and indication of future directions.

Predictions

A number of predictions follow from our model. Certain of these such as higher input produces higher output is not surprising and should only be regarded as confirmation of model and experiment. Other predictions such as the nature and quality of time courses also fit into the category of confirmation with previous work. On the other hand, our model predicts an IAP oscillation, Figure 1f, which to our knowledge is new. A more striking set of predictions follows from our exploration of DNA damage. Certainly the sigmoidal character of DNA fragmentation shown in Figure 2b represents a specific prediction that may be tested in the laboratory. Of greater interest and in the same vein is the prediction that duration of applied TNF-α can dramatically change the survival prospects of a cell. This was

shown in Figure 2b. Again this represents an experimentally refutable claim of our model.

It is uncertain whether the oscillations discovered by Hoffmann et al. (2002) are an important property of cellular behavior or an epi-phenomenon (Barken et al., 2005; Nelson et al., 2005). In any case, it is of interest to have a clear understanding of when these do and do not occur. Our model makes a series of predictions in this regard most of which are shown graphically in Figure 5. The prediction of a straight line locus based on the ratio of initial concentrations of FADD to IKK as a determinant of the presence or absence of oscillations is certainly an experimentally verifiable result. It is not clear how one might experimentally manipulate the delay time of transcription. Thus, the prediction of our model of lower and upper bounds of delay for the appearance of oscillations must await the appearance of a clever experimental technique.

Future Directions

It has been our goal in this article to create a parsimonious model of the pathways and phenomena which result from cellular stimulation by TNF-α. In so doing, we have turned our backs on important details. However, many of these details can be incorporated and used to expand the current model. In this section, we highlight some considerations that include detailed biological process and increase model complexity.

- Detailed and extended models of nuclear transcription: Hoffman et al. (2002) constructed a relatively detailed model of nuclear transcription engendered by NF-κB and this model was further investigated by Nelson et al. (2004). Other models for transcription as developed in Lee and Bailey (1984) can be applied to our model to incorporate the details of transcription.
- Extend the model to include responses to other stimuli: recent studies have studied the response of lipopolysaccharide-induced NF-κB (Covert et al., 2005) and stimulus specificity of gene expression programs (Werner et al., 2005). Our model can be extended to incorporate these different phenomena.
- Models of the various isoforms of IκB: as noted earlier in a footnote, there are three known isoforms of IκB that figure in the cytosolic sequestration of NF-κB. Our present model may be easily extended with the inclusion of the two additional isoforms as two additional modules (Hoffmann et al., 2002; Kearns et al., 2006).
- Incorporation of mitochondrial apoptotic pathway and the nuclear events associated with apoptosis: the nuclear events of apoptosis include chromatin condensation, DNA fragmentation, and budding of apoptotic bodies. The DNA repair associated enzyme poly (ADP-ribose) polymerase (PARP) can be cleaved by caspase-3, thereby hindering DNA repair and promoting DNA fragmentation. It is possible to extend our model to include further details of stress-induced and ligand-mediated apoptosis

to give a more complete representation (Fussenegger et al., 2000; Hua et al., 2005).

- Stochastic models to study fluctuations: our analysis applies to individual cells as pointed out by a referee for NF-κB ≈ 1 nM, this corresponds to ≈ 120 molecules which suggests a fluctuation of 10%, which may be regarded as tolerable, but stochasticity is an issue. Since Einstein's work, (Gardiner, 1997), we know that single unit dynamics provides the basis for stochastic formulation. In the present case, see Hayot and Jayaprakash (2006).
- Population dynamics: single cell dynamics can also be extended to population activity by means of statistical mechanics (Knight et al., 1996; Omurtag et al., 2000). Nelson et al. (2004), who show cell synchrony in response to NF-κB stimulation raise the issue of whether this might be a signaling tool and the related issues of synchrony and asynchrony amongst cells. It has been shown that a threshold of intercellular interaction is required before asynchrony turns to phase-locked synchrony—and that time lag restrains synchrony from running away (Sirovich et al., 2006).
- Analysis of results: further analysis of results may pinpoint causal relations which give rise to time histories and their phasic relations and provide an analytic basis for the locii of oscillation boundaries.
- Parametric sensitivity analysis: parametric sensitivity analysis may identify system parameters that are most sensitive to perturbation (Stelling et al., 2004). In this case, see Cho et al. (2003a).

Appendix

The Mathematical Model

In formulating the mathematical model we follow the approach presented (Sirovich and Rangamani, 2006). Under this approach, the model is fully specified by Figure 6, and the definitions of the fluxes, J, as given in Table I. Figure 6, although it has a superficial resemblance to the customary caricatures of biochemical systems, has in fact much more informational content and is quantitatively equivalent to the mathematical description of the system. The reader should note that in customary practice individual terms such as $k_1 c_1 c_2$ in J_1 of Table I are termed as a "flux" (Famili and Palsson, 2003). However, the only way this term occurs is in form J_1. In addition, in Figure 1, a flux J_n is reckoned positive if entering a concentration box and negative if exiting. Finally, the derivative of a concentration $dc_m/dt = c_m$ is equal to the sum of fluxes to its box. Thus if $c = [c_1, c_2, \ldots c_{31}]^+$, and $J = [J_1, J_2, \ldots J_{19}]^+$,

$$\frac{dc}{dt} = SJ \tag{1}$$

is the system, where S, having entries $0, \pm 1$, which we term stoichiometric matrix is shown in tabular form in Table V. The explicit form of Equation (1) is given in Table II. As a result of our definition of J, S is not the customary definition (Famili and Palsson, 2003). In a genuine sense, S is the embodiment of Figure 6.

One easily sees that (Sirovich and Rangamani, 2006), that there exists a matrix L, of zeros and ± 1, having 12 rows and 30 columns, such that

$$\frac{d}{dt} Lc = 0 \tag{2}$$

giving the invariants. One can show that S has an empty right null space and as a result at equilibrium, $J = 0$ is a necessary and sufficient condition. Equation (1) is equivalent to the specific form of the model given in Appendix.

For the convenience of the reader, S and L are represented in tabular form in Tables V and VI. The

Table III. Species and their initial values. The initial values of the participating chemical species are obtained from (Cho et al., 2003a; Eissing et al., 2004; Lipniacki et al., 2004).

Name	Species	Initial value (nM)
c_1	TNF-α	a
c_2	TNFR1	100
c_3	TNF-α/TNFR1	0
c_4	TRADD	150
c_5	TNF-α/TNFR1/TRADD	0
c_6	TRAF2	100
c_7	TNF-α/TNFR1/TRADD/TRAF2	0
c_8	RIP-1	100
c_9	TNF-α/TNFR1/TRADD/TRAF2/RIP-1[a]	0
c_{10}	IKK	100
c_{11}	TNF-α/TNFR1/TRADD/TRAF2/RIP-1/IKK[b]	0
c_{12}	IKK*	0
c_{13}	Iκ-B/NF-κB	250
c_{14}	Iκ-B/NF-κB/IKK*	0
c_{15}	Iκ-B-P	0
c_{16}	NF-κB	0
c_{17}	FADD	100
c_{18}	TNF-α/TNFR1/TRADD/TRAF2/RIP-1/FADD	0
c_{19}	TRADD/TRAF2/RIP-1/FADD	0
c_{20}	Caspase-8	80
c_{21}	TRADD/TRAF2/RIP-1/FADD/caspase-8[c]	0
c_{22}	Caspase-8*	0
c_{23}	Caspase-3	200
c_{24}	Caspase-8*/caspase-3	0
c_{25}	Caspase-3*	0
c_{26}	DNA-fragmentation	0
c_{27}	c-IAP	0
c_{28}	Caspase-3*/c-IAP	0
c_{29}	DNA (intact)	800
c_{30}	Caspase-3*/DNA	0
c_{31}	IκB	0

"a" represents the initial concentration of TNF-α, the control parameter.
[a]Early complex.
[b]Survival complex.
[c]Death complex (death-inducing signaling complex—DISC).

Table IV. Kinetic parameters (concentration is in nM and time in seconds).

Kinetic Parameter	Value $\times 10^3$	Kinetic parameter	Value $\times 10^3$
k_1	0.185	k_{15}	0.185
k_2	0.00125	k_{16}	0.00125
k_3	0.185	k_{17}	0.37
k_4	0.00125	k_{18}	0.5
k_5	0.185	k_{19}	0.2
k_6	0.00125	k_{20}	0.1
k_7	0.185	k_{21}	0.1
k_8	0.00125	k_{22}	0.06
k_9	0.185	k_{23}	100
k_{10}	0.00125	k_{24}	0.185
k_{11}	0.37	k_{25}	0.00125
k_{12}	0.014	k_{26}	0.37
k_{13}	0.00125	k_{27}	0.37
k_{14}	0.37	k_{28}	0.5
p	1.75	k_{29}	750

The first order rate constants have units of s^{-1} and the second order rate constants have units of $nM^{-1} \cdot s^{-1}$.

invariants obtained from L are presented below, with "a" representing the initial concentration of TNF-α. The invariants shown here are for the initial conditions shown in Table III.

Table V. Stoichiometric matrix S.

	J_1	J_2	J_3	J_4	J_5	J_6	J_7	J_8	J_9	J_{10}	J_{11}	J_{12}	J_{13}	J_{14}	J_{15}	J_{16}	J_{17}	J_{18}	J_{19}
c_1	−1	0	0	0	0	0	0	0	0	0	0	0	0	0	0	0	0	0	0
c_2	−1	0	0	0	0	1	0	0	0	1	0	0	0	0	0	0	0	0	0
c_3	1	−1	0	0	0	0	0	0	0	0	0	0	0	0	0	0	0	0	0
c_4	0	−1	0	0	0	1	0	0	0	0	0	1	0	0	0	0	0	0	0
c_5	0	1	−1	0	0	0	0	0	0	0	0	0	0	0	0	0	0	0	0
c_6	0	0	−1	0	0	1	0	0	0	0	0	0	1	0	0	0	0	0	0
c_7	0	0	0	1	−1	0	0	0	0	0	0	0	0	0	0	0	0	0	0
c_8	0	0	0	−1	0	1	0	0	0	0	0	0	1	0	0	0	0	0	0
c_9	0	0	0	1	−1	0	0	0	−1	0	0	0	0	0	0	0	0	0	0
c_{10}	0	0	0	0	−1	0	0	1	0	0	0	0	0	0	0	0	0	0	0
c_{11}	0	0	0	0	1	−1	0	0	0	0	0	0	0	0	0	0	0	0	0
c_{12}	0	0	0	0	0	1	−1	0	0	0	0	0	0	0	0	0	0	0	0
c_{13}	0	0	0	0	0	0	−1	0	0	0	0	0	0	0	0	0	0	0	1
c_{14}	0	0	0	0	0	0	1	−1	0	0	0	0	0	0	0	0	0	0	0
c_{15}	0	0	0	0	0	0	0	1	0	0	0	0	0	0	0	0	0	0	0
c_{16}	0	0	0	0	0	0	0	1	0	0	0	0	0	0	0	0	0	0	−1
c_{17}	0	0	0	0	0	0	0	0	−1	0	0	1	0	0	0	0	0	0	0
c_{18}	0	0	0	0	0	0	0	0	1	−1	0	0	0	0	0	0	0	0	0
c_{19}	0	0	0	0	0	0	0	0	0	1	−1	0	0	0	0	0	0	0	0
c_{20}	0	0	0	0	0	0	0	0	0	0	−1	0	0	0	0	0	0	0	0
c_{21}	0	0	0	0	0	0	0	0	0	0	1	−1	0	0	0	0	0	0	0
c_{22}	0	0	0	0	0	0	0	0	0	0	0	1	−1	1	0	0	0	0	0
c_{23}	0	0	0	0	0	0	0	0	0	0	0	0	−1	0	0	0	0	0	0
c_{24}	0	0	0	0	0	0	0	0	0	0	0	0	1	−1	0	0	0	0	0
c_{25}	0	0	0	0	0	0	0	0	0	0	0	0	0	1	−1	1	0	−1	0
c_{26}	0	0	0	0	0	0	0	0	0	0	0	0	0	0	1	0	0	0	0
c_{27}	0	0	0	0	0	0	0	0	0	0	0	0	0	0	0	1	−1	0	0
c_{28}	0	0	0	0	0	0	0	0	0	0	0	0	0	0	0	0	1	0	0
c_{29}	0	0	0	0	0	0	0	0	0	0	0	0	0	0	−1	0	0	0	0
c_{30}	0	0	0	0	0	0	0	0	0	0	0	0	0	0	1	−1	0	0	0
c_{31}	0	0	0	0	0	0	0	0	0	0	0	0	0	0	0	1	0	−1	0

Table VI. Left null space of the stoichiometric matrix, L.

	1	2	3	4	5	6	7	8	9	10	11	12
c_1	0	0	0	0	0	0	−1	0	1	1	−1	0
c_2	0	0	0	0	0	1	1	−1	0	0	0	0
c_3	0	0	0	0	0	1	0	−1	1	1	−1	0
c_4	−1	−1	0	0	−1	0	0	1	−1	−1	1	0
c_5	−1	−1	0	0	−1	1	0	0	0	0	0	0
c_6	1	0	0	0	0	0	0	0	0	0	0	0
c_7	0	−1	0	0	−1	1	0	0	0	0	0	0
c_8	0	1	0	0	0	0	0	0	0	0	0	0
c_9	0	0	0	0	−1	1	0	0	0	0	0	0
c_{10}	0	0	1	−1	0	0	1	0	−1	−1	1	−1
c_{11}	0	0	1	−1	−1	1	1	0	−1	−1	1	−1
c_{12}	0	0	1	−1	0	0	0	0	0	0	0	−1
c_{13}	0	0	0	1	0	0	0	0	0	0	0	1
c_{14}	0	0	1	0	0	0	0	0	0	0	0	0
c_{15}	0	0	0	0	0	0	−1	0	1	1	−1	1
c_{16}	0	0	0	1	0	0	0	0	0	0	0	0
c_{17}	0	0	0	0	1	0	0	0	0	0	0	0
c_{18}	0	0	0	0	0	1	0	0	0	0	0	0
c_{19}	0	0	0	0	0	0	−1	1	0	0	0	0
c_{20}	0	0	0	0	0	0	1	0	0	0	0	0
c_{21}	0	0	0	0	0	0	0	1	0	0	0	0
c_{22}	0	0	0	0	0	0	0	0	1	1	−1	0
c_{23}	0	0	0	0	0	0	0	0	0	−1	1	0
c_{24}	0	0	0	0	0	0	0	0	1	0	0	0
c_{25}	0	0	0	0	0	0	0	0	0	−1	1	0
c_{26}	0	0	0	0	0	0	0	0	1	0	0	0
c_{27}	0	0	0	0	0	0	0	0	0	0	0	−1
c_{28}	0	0	0	0	0	0	0	0	0	−1	1	−1
c_{29}	0	0	0	0	0	0	0	0	1	0	0	0
c_{30}	0	0	0	0	0	0	0	0	0	0	1	0
c_{31}	0	0	0	0	0	0	0	0	0	0	0	1

Invariants

(1) $-c_4 - c_5 + c_6 = -50$

(2) $-c_4 - c_5 + c_8 - c_7 = -50$

(3) $c_{10} + c_{12} + c_{14} + c_{11} = 100$

(4) $c_{16} - c_{10} + c_{13} - c_{12} - c_{11} = 150$

(5) $-c_4 - c_5 - c_7 - c_9 + c_{17} - c_{11} = -50$

(6) $c_2 + c_5 + c_7 + c_{18} + c_9 + c_{11} + c_3 = 100$

(7) $-c_1 + c_2 + c_{20} - c_{15} + c_{10} - c_{19} + c_{11} = 280 - a$

(8) $c_4 - c_2 + c_{21} + c_{19} - c_3 = 50$

(9) $-c_4 + c_1 + c_{15} - c_{10} + c_{24} + c_{22} - c_{11} + c_3 = -250 + a$

(10) $-c_4 + c_1 + c_{15} - c_{10} + c_{26} + c_{29} - c_{23} - c_{25} + c_{22} - c_{28} - c_{11} + c_3 = 350 + a$

(11) $c_{26} + c_{30} + c_{29} = 800$

(12) $c_{15} - c_{10} + c_{31} + c_{13} - c_{27} - c_{12} - c_{28} - c_{11} = 150$

References

Barken D, Wang CJ, Kearns J, Cheong R, Hoffmann A, Levchenko A. 2005. Comment on ''Oscillations in NF-kappaB signaling control the dynamics of gene expression''. Science 308(5718):52a.

Barnhart BC, Peter ME. 2003. The TNF receptor 1: A split personality complex. Cell 114(2):148–150.

Baud V, Karin M. 2001. Signal transduction by tumor necrosis factor and its relatives. Trends Cell Biol 11(9):372–377.

Callard RE, Yates AJ. 2005. Immunology and mathematics: Crossing the divide. Immunology 115(1):21–33.

Cho KH, Shin SY, Kolch W, Wolkenhauer O. 2003a. Experimental design in systems biology, based on parameter sensitivity analysis using a Monte Carlo method: A case study for the TNF-alpha mediated NF-kappaB signal transduction pathway. Simulation 79:726–739.

Cho KH, Shin SY, Lee HW, Wolkenhauer O. 2003b. Investigations into the analysis and modeling of the TNF alpha-mediated NF-kappa B-signaling pathway. Genome Res 13(11):2413–2422.

Covert MW, Leung TH, Gaston JE, Baltimore D. 2005. Achieving stability of lipopolysaccharide-induced NF-κB activation. Science 309(5742):1854–1857.

Delhalle S, Blasius R, Dicato M, Diederich M. 2004. A beginner's guide to NF-kappaB signaling pathways. Ann NY Acad Sci 1030:1–13.

Eissing T, Conzelmann H, Gilles ED, Allgower F, Bullinger E, Scheurich P. 2004. Bistability analyses of a caspase activation model for receptor-induced apoptosis. J Biol Chem 279(35):36892–36897.

Famili I, Palsson BO. 2003. The convex basis of the left null space of the stoichiometric matrix leads to the definition of metabolically meaningful pools. Biophys J 85(1):16–26.

Fussenegger M, Bailey JE, Varner J. 2000. A mathematical model of caspase function in apoptosis. Nat Biotechnol 18(7):768–774.

Gardiner GW. 1997. Handbook of stochastic methods. Berlin, Heidelberg: Springer.

Greten FR, Karin M. 2004. The IKK/NF-κB activation pathway-a target for prevention and treatment of cancer. Cancer Lett 206(2):193–199.

Hayot F, Jayaprakash C. 2006. NF-κB oscillations and cell-to-cell variability. J Theor Biol 240(4):583–591.

Hoffmann A, Levchenko A, Scott ML, Baltimore D. 2002. The IκB-NF-κB signaling module: Temporal control and selective gene activation. Science 298(5596):1241–1245.

Holcik M, Korneluk RG. 2001. XIAP, the guardian angel. Nat Rev Mol Cell Biol 2(7):550–556.

Hua F, Cornejo MG, Cardone MH, Stokes CL, Lauffenburger DA. 2005. Effects of Bcl-2 levels on Fas signaling-induced caspase-3 activation: Molecular genetic tests of computational model predictions. J Immunol 175(2):985–995.

Ioannou YA, Chen FW. 1996. Quantitation of DNA fragmentation in apoptosis. Nucleic Acids Res 24(5):992–993.

Jin Z, El-Deiry WS. 2005. Overview of cell death signaling pathways. Cancer Biol Ther 4(2):139–163.

Karin M, Yamamoto Y, Wang QM. 2004. The IKK NF-κB system: A treasure trove for drug development. Nat Rev Drug Discov 3(1):17–26.

Kearns JD, Basak S, Werner SL, Huang CS, Hoffmann A. 2006. Ikappa-Bepsilon provides negative feedback to control NF-kappaB oscillations, signaling dynamics, and inflammatory gene expression. J Cell Biol 173(5):659–664.

Knight B, Manin D, Sirovich L. 1996. Dynamical models of interacting neuron populations in visual cortex. In: Gerf EC, editor. Symposium on Robotics and Cybernetics: Computational Engineering in Systems Applications. Lille, France: Cite Scientifique.

Lee SE, Bailey JE. 1984. Genetically structured models for lac promoter-operator function in the Escherichia coli chromosome and in multicopy plasmids: Lac operator function. Biotech Bioeng 26(11):1372–1382.

Lipniacki T, Paszek P, Brasier AR, Luxon B, Kimmel M. 2004. Mathematical model of NF-κB regulatory module. J Theor Biol 228(2):195–215.

Liston P, Young SS, Mackenzie AE, Korneluk RG. 1997. Life and death decisions: The role of the IAPs in modulating programmed cell death. Apoptosis 2(5):423–441.

Luo JL, Kamata H, Karin M. 2005. IKK/NF-κB signaling: Balancing life and death—a new approach to cancer therapy. J Clin Invest 115(10):2625–2632.

McDunn JE, Cobb JP. 2005. That which does not kill you makes you stronger: A molecular mechanism for preconditioning. Sci STKE 291:34.

Micheau O, Tschopp J. 2003. Induction of TNF receptor I-mediated apoptosis via two sequential signaling complexes. Cell 114(2):181–190.

Nelson DE, Ihekwaba AE, Elliott M, Johnson JR, Gibney CA, Foreman BE, Nelson G, See V, Horton CA, Spiller DG. 2004. Oscillations in NF-kappaB signaling control the dynamics of gene expression. Science 306(5696):704–708.

Nelson DE, Horton CA, See V, Johnson JR, Nelson G, Spiller DG, Kell DB, White MR. 2005. Response to Comment on ''Oscillations in NF-{kappa}B signaling control the dynamics of gene expression''. Science 308:52b.

Omurtag A, Knight BW, Sirovich L. 2000. On the simulation of large populations of neurons. J Comput Neurosci 8(1):51–63.

Papa S, Zazzeroni F, Pham CG, Bubici C, Franzoso G. 2004. Linking JNK signaling to NF-κB: A key to survival. J Cell Sci 117(Pt 22):5197–5208.

Polunovsky VA, Wendt CH, Ingbar DH, Peterson MS, Bitterman PB. 1994. Induction of endothelial cell apoptosis by TNF alpha: Modulation by inhibitors of protein synthesis. Exp Cell Res 214(2):584–594.

Popper KP. 2002. The logic of scientific discovery. Great Britain: Routledge.

Rehm M, Dussmann H, Janicke RU, Tavare JM, Kogel D, Prehn JH. 2002. Single-cell fluorescence resonance energy transfer analysis demonstrates that caspase activation during apoptosis is a rapid process. Role of caspase-3. J Biol Chem 277(27):24506–24514.

Schneider P, Tschopp J. 2000. Modulation of death receptor signalling. Symp Soc Exp Biol 52:31–42.

Schottelius AJ, Moldawer LL, Dinarello CA, Asadullah K, Sterry W, Edwards CK. 2004. Biology of tumor necrosis factor-alpha-implications for psoriasis. Exp Derm 13(4):193–222.

Shi Y. 2002. Mechanisms of caspase activation and inhibition during apoptosis. Mol Cell 9(3):459–470.

Sirovich L, Rangamani P. 2006. Mathematical Analysis of Biochemical Pathways: Application to TNF-alpha Signaling. http://camelot.mssm.edu/publications/publications.html.

Sirovich L, Omurtag A, Lubliner K. 2006. Dynamics of neural populations: Stability and synchrony. Network 17(1):3–29.

Stelling J, Gilles ED, Doyle FJ, III . 2004. From the cover: Robustness properties of circadian clock architectures. Proc Natl Acad Sci USA 101(36):13210–13215.

Sung MH, Simon R. 2004. In silico simulation of inhibitor drug effects on nuclear factor-κB pathway dynamics. Mol Pharmacol 66(1):70–75.

Wajant H, Pfizenmaier K, Scheurich P. 2003. Tumor necrosis factor signaling. Cell Death Diff 10(1):45–65.

Wallach D. 1997. Cell death induction by TNF: A matter of self control. Trends Biochem Sci 22(4):107–109.

Wallach D, Kovalenko AV, Varfolomeev EE, Boldin MP. 1998. Death-inducing functions of ligands of the tumor necrosis factor family: A Sanhedrin verdict. Curr Opin Immunol 10(3):279–288.

Wang CY, Mayo MW, Baldwin AS, Jr . 1996. TNF-α and cancer therapy-induced apoptosis: Potentiation by inhibition of NF-kappaB. Science 274(5288):784–787.

Wang F, Chen TS, Xing D, Wang JJ, Wu YX. 2005. Measuring dynamics of caspase-3 activity in living cells using FRET technique during apoptosis induced by high fluence low-power laser irradiation. Lasers Surg Med 36(1):2–7.

Werner SL, Barken D, Hoffmann A. 2005. Stimulus specificity of gene expression programs determined by temporal control of IKK activity. Science 309(5742):1857–1861.

Wright SC, Kumar P, Tam AW, Shen N, Varma M, Larrick JW. 1992. Apoptosis and DNA fragmentation precede TNF-induced cytolysis in U937 cells. J Cell Biochem 48(4):344–355.